

# Electrochemical Nucleation of Stable N<sub>2</sub> Nanobubbles at Pt Nanoelectrodes

Qianjin Chen,<sup>†</sup> Hilke S. Wiedenroth,<sup>†,‡</sup> Sean R. German,<sup>†,§</sup> and Henry S. White<sup>\*,†</sup>

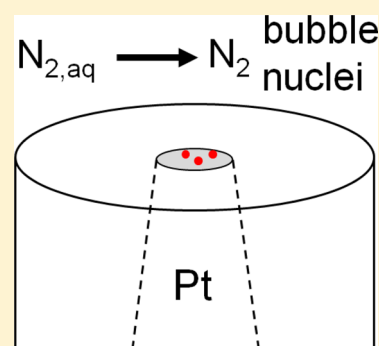
<sup>†</sup>Department of Chemistry, University of Utah, 315 S 1400 E, Salt Lake City, Utah 84112, United States

<sup>‡</sup>Department of Environmental and Sustainable Chemistry, Braunschweig University of Technology, Hagenring 30, Braunschweig 38106, Germany

<sup>§</sup>Revalerio Corporation, 1200 East D Street, Tacoma, Washington 98421, United States

**S** Supporting Information

**ABSTRACT:** Exploring the nucleation of gas bubbles at interfaces is of fundamental interest. Herein, we report the nucleation of individual N<sub>2</sub> nanobubbles at Pt nanodisk electrodes (6–90 nm) via the irreversible electrooxidation of hydrazine (N<sub>2</sub>H<sub>4</sub> → N<sub>2</sub> + 4H<sup>+</sup> + 4e<sup>-</sup>). The nucleation and growth of a stable N<sub>2</sub> nanobubble at the Pt electrode is indicated by a sudden drop in voltammetric current, a consequence of restricted mass transport of N<sub>2</sub>H<sub>4</sub> to the electrode surface following the liquid-to-gas phase transition. The critical surface concentration of dissolved N<sub>2</sub> required for nanobubble nucleation, C<sub>N<sub>2</sub>,critical</sub><sup>S</sup>, obtained from the faradaic current at the moment just prior to bubble formation, is measured to be ~0.11 M and is independent of the electrode radius and the bulk N<sub>2</sub>H<sub>4</sub> concentration. Our results suggest that the size of stable gas bubble nuclei depends only on the local concentration of N<sub>2</sub> near the electrode surface, consistent with previously reported studies of the electrogeneration of H<sub>2</sub> nanobubbles. C<sub>N<sub>2</sub>,critical</sub><sup>S</sup> is ~160 times larger than the N<sub>2</sub> saturation concentration at room temperature and atmospheric pressure. The residual current for N<sub>2</sub>H<sub>4</sub> oxidation after formation of a stable N<sub>2</sub> nanobubble at the electrode surface is proportional to the N<sub>2</sub>H<sub>4</sub> concentration as well as the nanoelectrode radius, indicating that the dynamic equilibrium required for the existence of a stable N<sub>2</sub> nanobubble is determined by N<sub>2</sub>H<sub>4</sub> electrooxidation at the three phase contact line.



## INTRODUCTION

Gas bubbles at solid interfaces are an important research area in surface chemistry, physics, nanofluidics, and chemical engineering. Investigations focus on unraveling the mystery behind bubble nucleation,<sup>1–8</sup> quantifying bubble dynamics as a function of different parameters,<sup>9–11</sup> as well as developing potential applications of nanobubbles in lubrication,<sup>12</sup> cleaning,<sup>13</sup> and synthesizing highly porous metallic surfaces.<sup>14</sup> It has been proposed that interfacial nanobubbles result from a supersaturation of gas at the solid/liquid interface,<sup>1,2</sup> which can be realized by solvent exchange,<sup>9,10</sup> substrate heating,<sup>11,15</sup> or solution decompression.<sup>5–7</sup> Supersaturated solutions are not at equilibrium due to the energy barrier required to form a gas bubble. Upon nucleation, energy is released when dissolved gas molecules at a high chemical potential nucleate a gas phase at a lower partial potential, while formation of a bubble requires additional energy to maintain the surface.<sup>3</sup> In practice, there is a large discrepancy between classical homogeneous nucleation theories and experimental results.<sup>4</sup> For example, theories predict that the threshold concentration of gas needed to cause nucleation should be essentially independent of the gas species used, while experiments demonstrate the opposite.<sup>5–7</sup>

Existence of interfacial nanobubbles and their physical properties is supported by studies using atomic force microscopy in tapping mode (TM-AFM).<sup>8–10,16,17</sup> Several

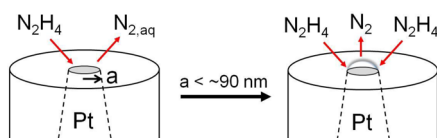
mechanisms have been proposed to explain the long lifetime of surface nanobubbles, including the role of impurities on the bubble surface,<sup>18</sup> dynamic equilibrium,<sup>19</sup> and contact line pinning,<sup>20,21</sup> but still no general agreement has been reached. Recently, electrochemical experiments have advanced fundamental studies of gas nanobubbles, since high overpotentials will readily lead to supersaturation of the solution near the electrode with electrogenerated gas, resulting in heterogeneous nucleation. Bubbles of hydrogen or oxygen from water electrolysis at a gas-evolving electrode were first imaged by photography<sup>22–24</sup> and now by AFM with nanoscopic resolution.<sup>16,17,25</sup> Instead of generating a large ensemble of bubbles on a macroscopic electrode surface, a single nanobubble can also be generated on small electrode surfaces. Recently, we reported the electrogeneration of individual H<sub>2</sub> nanobubbles at Pt nanodisk electrodes with radii <50 nm via the reduction of protons.<sup>26–28</sup> We find that H<sub>2</sub> nanobubble nucleation at the Pt disk electrode occurs at a constant H<sub>2</sub> supersaturation concentration, independent of the electrode size and proton source. These nanobubbles are stabilized by a dynamic equilibrium between the H<sub>2</sub> diffusive outflux and the electrogeneration of H<sub>2</sub> at the three-phase boundary.

Received: July 9, 2015

Published: August 31, 2015

Herein, we focus on the electrochemical generation of N<sub>2</sub> nanobubbles from electrooxidation of hydrazine (N<sub>2</sub>H<sub>4</sub>) on Pt disk nanoelectrodes. N<sub>2</sub>H<sub>4</sub> oxidation is of importance in the fields of electroanalysis and electrocatalysis, and the mechanism and kinetics of N<sub>2</sub>H<sub>4</sub> oxidation on Pt electrodes have received renewed attention recently.<sup>29–32</sup> In single-particle collision experiments, an electrocatalytic current arises when a single Pt nanoparticle collides with the relatively inactive Au,<sup>33,34</sup> Ni,<sup>35</sup> boron-doped diamond,<sup>36</sup> or carbon-fiber<sup>37</sup> electrode to electrocatalyze N<sub>2</sub>H<sub>4</sub> oxidation. The observed “blip” response of the current at a high overpotential is attributed to the deactivation of the Pt nanoparticles, although the possibility of N<sub>2</sub> nanobubble formation has been recently suggested.<sup>35</sup> In the current article, we use Pt disk nanoelectrodes (<90 nm radius) to study N<sub>2</sub>H<sub>4</sub> electrooxidation and demonstrate that single nanobubbles of N<sub>2</sub> indeed can be electrochemically generated at the Pt nanoelectrodes (Scheme 1). We further measure the

**Scheme 1. Schematic Drawing of the Electrochemical Formation of a Single N<sub>2</sub> Bubble from N<sub>2</sub>H<sub>4</sub> Electrooxidation at a Pt Nanodisk Electrode with a Radius of  $a < \sim 90$  nm**



critical concentration of the dissolved gas required for nanobubble nucleation,  $\sim 0.11$  M, corresponding to a value that is  $\sim 160$  times larger than the corresponding N<sub>2</sub> saturation concentration at room temperature and atmospheric pressure. The results for N<sub>2</sub> nanobubble nucleation and stability are qualitatively analogous to that for H<sub>2</sub> nanobubble from proton reduction in sulfuric acid solution.<sup>26,27</sup>

## EXPERIMENTAL SECTION

Sulfuric acid (Mallinckrodt, 96.2%, ACS grade) and N<sub>2</sub>H<sub>4</sub> (Aldrich, 35 wt % in water stored under N<sub>2</sub>) were used as received. All aqueous solutions were prepared from deionized water (18.2 M $\Omega$ ·cm) and were bubbled with N<sub>2</sub> gas to remove dissolved O<sub>2</sub>. As shown below, the saturation concentration of dissolved N<sub>2</sub> in the solution at room temperature and ambient pressure ( $\sim 0.69$  mM), resulting from bubbling, is  $\sim 0.6\%$  of the concentration required for bubble nucleation. N<sub>2</sub>H<sub>4</sub> solutions were freshly prepared daily to reduce the effect of autodecomposition.<sup>38</sup>

Pt nanodisk electrodes were fabricated according to previously reported procedures from our laboratory.<sup>39</sup> Details can be found in the literature as well as our previous reports.<sup>26,28</sup> In order to prepare circular nanodisk electrodes, the electrochemically sharpened Pt wires were carefully aligned along the glass capillaries and then sealed within the glass in H<sub>2</sub> flame.<sup>39</sup> The radii of the nanodisk electrodes,  $a$ , were determined from the voltammetric steady-state diffusion-limited current,  $i_{\text{lim}}$ , for the oxidation of ferrocene ( $\text{Fc} \rightarrow \text{Fc}^+ + \text{e}^-$ ) dissolved in acetonitrile (CH<sub>3</sub>CN) containing 0.10 M tetrabutylammonium hexafluorophosphate (TBAPF<sub>6</sub>). The radii were calculated using the equation:<sup>40,41</sup>

$$i_{\text{lim}} = 4nFD_{\text{Fc}}C_{\text{Fc}}^*a \quad (1)$$

where  $D_{\text{Fc}}$  ( $2.4 \times 10^{-5}$  cm<sup>2</sup>/s)<sup>42</sup> and  $C_{\text{Fc}}^*$  (3.25 mM) are the diffusion coefficient and the bulk concentration of Fc, respectively, and  $n$  is the number of electrons transferred per molecule ( $= 1$  for Fc oxidation). Experimental steady-state voltammograms for measuring the electrode radii are presented in Figure S1 in the Supporting Information.

A Dagan Cornerstone Chem-Clamp potentiostat and a Pine RDE4 (used as waveform generator) were interfaced to a computer through a PCI data acquisition card (National Instruments) to collect  $i$ - $V$  data. A Ag/AgCl (in 3 M NaCl) electrode and a saturated calomel electrode (SCE) were used as the counter/reference electrode in a two-electrode cell configuration.

## RESULTS AND DISCUSSION

Single N<sub>2</sub> nanobubble formation is observed at Pt nanodisk electrodes of radius <90 nm during the oxidation of N<sub>2</sub>H<sub>4</sub> when the bulk concentration of N<sub>2</sub>H<sub>4</sub> is  $\geq 0.30$  M. Figure 1a shows a

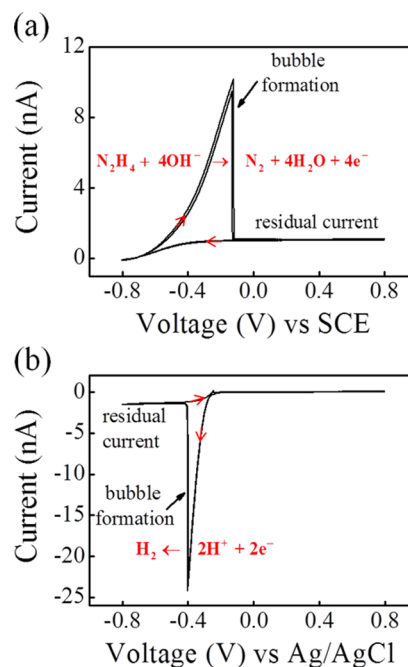


**Figure 1.**  $i$ - $V$  responses of a 32 nm-radius Pt nanoelectrode immersed in (a) 1.0 M N<sub>2</sub>H<sub>4</sub> and (b) 0.5 M H<sub>2</sub>SO<sub>4</sub> at a scan rate of 200 mV/s. The voltammograms shown are for two scan cycles. The initial potential is  $-0.80$  V in (a) and  $0.0$  V in (b), respectively, and the arrows indicate the direction of potential scanning.

typical cyclic voltammogram recorded at a 32 nm radius Pt nanodisk electrode immersed into a 1.0 M N<sub>2</sub>H<sub>4</sub> solution. At potentials positive of  $\sim -0.70$  V versus SCE, close to the thermodynamic potential for N<sub>2</sub>H<sub>4</sub> electrooxidation reaction at Pt electrodes,<sup>43</sup> the current associated with N<sub>2</sub>H<sub>4</sub> oxidation slowly rises, and the voltammetric shape is controlled by N<sub>2</sub>H<sub>4</sub> transport, ohmic loss, as well as the electron-transfer kinetics. The current increases until reaching a peak value,  $i_{\text{nb}}^{\text{p}}$ , of  $\sim 10$  nA, and then suddenly drops to a stable residual current of  $\sim 1.0$  nA. We ascribed this peak-shaped characteristic waveshape to the formation of a single gas nanobubble at the electrode surface. For comparison, the voltammetric response corresponding to single H<sub>2</sub> bubble formation, using the same electrode immersed into a 0.5 M H<sub>2</sub>SO<sub>4</sub> solution, is shown in Figure 1b. Note that the voltammetric wave for N<sub>2</sub> bubble formation is drawn out in comparison to H<sub>2</sub> bubble, presumably because of slower electron-transfer kinetics.

After formation of the N<sub>2</sub> nanobubble, the current decreases to a small residual value,  $i_{\text{nb}}^{\text{r}}$ , which is very stable at potentials positive of the peak potential. The small  $i_{\text{nb}}^{\text{r}}$  value suggests that the gas nanobubble blocks most of the active Pt surface, reducing the rate of N<sub>2</sub>H<sub>4</sub> oxidation. We believe that  $i_{\text{nb}}^{\text{r}}$

corresponds to the rate of  $N_2$  electrogeneration at the electrode surface required to balance the  $N_2$  diffusive outflux from the bubble into the solution. Understanding the factors that control  $i_{nb}^p$  provides insight into the mechanism by which a nanobubble remains stable.

Surprisingly,  $i_{nb}^p$  for  $N_2$  bubbles is found to depend on the time that the Pt disk electrode is immersed into the  $N_2H_4$  solution. As typified for a 32 nm radius Pt disk electrode, the initial  $i_{nb}^p$  from voltammetric responses after a freshly prepared Pt electrode is immersed into the  $N_2H_4$  solution is  $\sim 10$  nA. As the immersion time increases while continuously scanning the electrode potential,  $i_{nb}^p$  decreases gradually and levels off to  $\sim 7$  nA after 10 min. Control experiments with the electrode disconnected from the cell circuit during the time intervals between two consecutive voltammetric measurements were also conducted, and a very similar decrease in  $i_{nb}^p$  was observed, indicating that potential scanning is not required to observe the current decrease. From the literature, the decrease of  $i_{nb}^p$  with immersion time is likely due to the known adsorption of  $N_2H_4$  and reaction intermediates at the Pt surface,<sup>44,45</sup> which inhibit the oxidation of  $N_2H_4$ , and further affects bubble nucleation. The recovery of  $i_{nb}^p$  can be achieved by careful rinsing the electrode with copious amounts of  $CH_3CN$  and water (see Supporting Information Figure S2), indicating weak adsorption of adsorbates. Figure 2 shows that the voltammetric response,

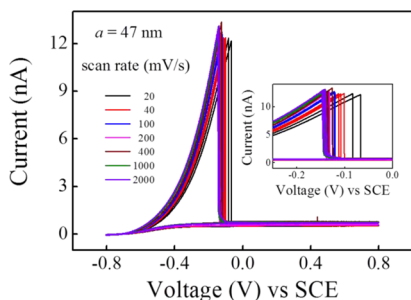


**Figure 2.** Cyclic voltammograms at different scan rates for a 47 nm-radius disk electrode in 1.0 M  $N_2H_4$  solution obtained at immersion times between 10 and 20 min. Little dependence of  $i_{nb}^p$  on the scan rate from 20 mV/s to 2.0 V/s is observed.

including the value of  $i_{nb}^p$ , is essentially independent of the scan rate between 20 mV/s to 2 V/s, indicating that the  $N_2$  concentration profile around the electrode surface reaches a steady state within this range of voltammetric scan rates. In quantifying the threshold gas concentration for  $N_2$  bubble nucleation, the initial value of  $i_{nb}^p$  for a pristine Pt electrode is believed to more accurately describe the nucleation supersaturation concentration. Thus, throughout the remainder of this paper,  $i_{nb}^p$  refers to the initial value obtained from averaging the peak current from voltammetric responses within the first five scan cycles after freshly rinsed electrodes are immersed into the  $N_2H_4$  solution.

Similar to previous results reported for  $H_2$  nanobubble formation, the appearance of a sharp peak in the voltammetric response occurs only at  $N_2H_4$  concentrations above a critical value. Below this value, the voltammetric response of the nanodisk electrode displays a sigmoidal shape that is characteristic of a diffusion-limited response without interference of a liquid-to-gas phase transition. Figure 3a shows voltammograms recorded at a 27 nm radius Pt nanodisk in  $N_2H_4$  solutions below the critical concentration (0.02, 0.05, 0.10, and 0.20 M)

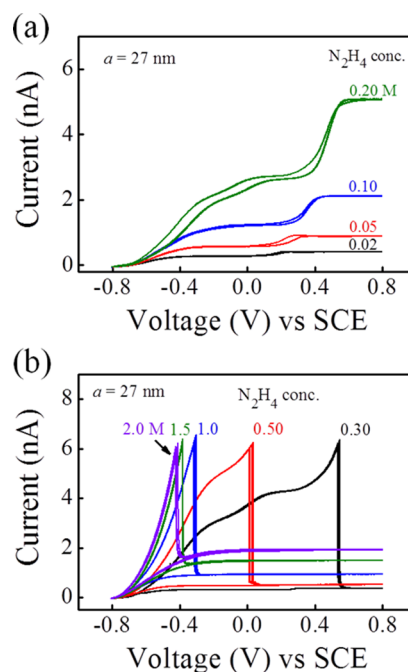
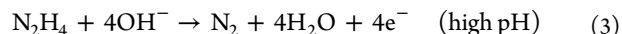
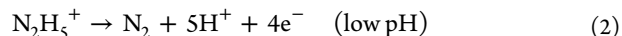


**Figure 3.**  $i$ - $V$  responses of a 27 nm radius Pt nanoelectrode immersed in (a) 0.02, 0.05, 0.10, and 0.20 M  $N_2H_4$ , where only sigmoidal-shaped waves are observed, and (b) 0.30, 0.50, 1.0, 1.5, and 2.0 M  $N_2H_4$ , where peak-shaped waves are observed, at a scan rate of 100 mV/s.

for bubble formation. Unlike the one step sigmoidal shape voltammetric response for proton reduction, the voltammograms for  $N_2H_4$  oxidation in the absence of bubble formation display two current plateaus in solutions containing 0.02, 0.05, and 0.10 M  $N_2H_4$  (and likely three current plateaus for 0.20 M  $N_2H_4$ ), indicating that the  $N_2H_4$  oxidation reaction at Pt nanoelectrodes is a multiple-step reaction with several redox-active intermediates. We find that the limiting current for both the plateau between 0.1 and 0.2 V and the plateau at 0.8 V increases approximately linearly with the  $N_2H_4$  concentration. From previous studies, it was concluded that  $N_2H_4$  electro-oxidation at Pt electrodes takes place as a stepwise electrochemical dehydrogenation process with dissolved  $N_2$  as the main product.<sup>46,47</sup> Different step reaction mechanisms and intermediates have been proposed, which vary both as a function of the nature and structure of the electrode surface and electrolyte composition/pH.<sup>30,48</sup>



Further discussion of hydrazine electrooxidation mechanism at Pt electrodes is beyond the scope of this paper and can be found in a comprehensive review elsewhere.<sup>48</sup> Given that the overall number of electrons transferred per  $N_2H_4$  molecule is 4, we obtain a diffusivity of  $6.1 \times 10^{-6}$  cm<sup>2</sup>/s from the limiting current of 5.07 nA at the 27 nm disk electrode in a 0.20 M  $N_2H_4$  solution ( $i_{lim} = 4nFDCA$ ), which lies within the range of reported values ( $0.5$ – $1.5 \times 10^{-5}$  cm<sup>2</sup>/s).<sup>36,46,49,50</sup>

Despite the complexity of the mechanism of  $N_2H_4$  oxidation, the key finding is that peak-shaped voltammetric responses are consistently observed in solutions containing a concentration of 0.30 M or greater, as demonstrated in Figure 3b. Remarkably, the  $N_2$  nanobubble peak current  $i_{nb}^p$  at the 27 nm radius disk electrode remains constant at  $\sim 6$  nA as the  $N_2H_4$  concentration

further increases, indicating that the bubble nucleation is determined by a critical  $N_2$  concentration at the electrode surface, rather than the concentration of  $N_2H_4$  available for oxidation. The multiple current plateaus before bubble formation for 0.30 and 0.50 M  $N_2H_4$  solutions, Figure 3, further suggest the stepwise  $N_2H_4$  electrooxidation reaction. The nanobubble peak potential shifts from 0.54 V for 0.30 M  $N_2H_4$  to a much lower potential of  $-0.42$  V for 2.0 M  $N_2H_4$ . The drawn out cyclic voltammogram at low  $N_2H_4$  concentration is analogous to that observed for the  $H_2$  bubble nucleation in a weak acid solution, e.g., acetic acid, as previously reported.<sup>26,27</sup> Additional overpotential drives the pre-equilibrium dissociation of the weak acid prior to proton reduction to allow sufficient  $H_2$  electrogeneration to nucleate a gas nanobubble. The large shift in the nanobubble peak potential with  $N_2H_4$  concentration suggests that  $N_2H_4$  electrooxidation is limited by electron-transfer kinetics, rather than mass transport. In summary, at low  $N_2H_4$  concentrations, the corresponding concentration of electrogenerated  $N_2$  at the electrode surface fails to achieve the value required for bubble nucleation, while at higher  $N_2H_4$  concentrations, the concentration of  $N_2$  molecules is sufficient to nucleate a nanobubble; this critical  $N_2$  concentration is independent of the bulk concentration of  $N_2H_4$ .

Since nanobubbles at interfaces are extremely sensitive to surfactants or contaminants,<sup>18</sup> ultrapure water was used as the electrolyte, and subsequently a significant ohmic drop occurs between the electrodes. To confirm that our results are not overly distorted by the solution resistance, a 1.0 M  $N_2H_4$  solution containing 0.20 M KCl as supporting electrolyte was also investigated. As shown in Figure 4, the cyclic voltam-

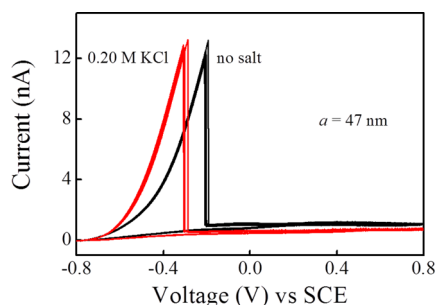


**Figure 4.** Cyclic voltammograms at 200 mV/s for a 47 nm radius disk electrode in 1.0 M  $N_2H_4$  with (red line) and without (black line) 0.20 M KCl as supporting electrolyte.

gram in the presence of 0.20 M KCl rises more steeply than without KCl, indicating that the drawn out wave in the absence of supporting electrolyte is partly due to the resistive drop between the electrodes. However, regardless of whether or not the solution contains a supporting electrolyte, the peak current corresponding to bubble formation remains constant, further confirming our hypothesis that a constant critical gas concentration for nucleation.

The residual current after bubble formation is also approximately the same after salt addition, consistent with previous electrochemical studies on  $H_2$  bubble formation, where no change of residual current was observed when inert salts (KCl,  $Na_2SO_4$ , sodium citrate) were added to the 0.5 M  $H_2SO_4$  solution.<sup>27</sup> Studies of the effects of salts on the interfacial nanobubble stability using TM-AFM also concluded

that surface nanobubbles, once formed, were insensitive to the addition of salts.<sup>10</sup>

We now consider the effect of Pt electrode radii on bubble nucleation. In the case of proton reduction, a peak shape voltammetric response corresponding to the  $H_2$  bubble formation is consistently observed only for nanodisks with radii  $< \sim 50$  nm, whereas for radii  $> \sim 50$  nm, a sigmoidal-shaped voltammetry with significant hysteresis is observed. The maximum Pt electrode radius to reproducibly form a  $N_2$  nanobubble is found to be  $\sim 90$  nm. Figure 5 shows typical

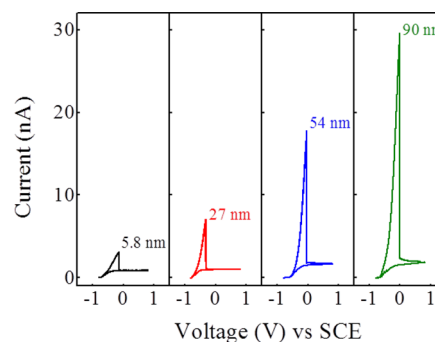


**Figure 5.**  $i$ - $V$  responses of Pt nanoelectrodes with radii of 5.8, 27, 54, and 90 nm in 1.0 M  $N_2H_4$  at a scan rate of 200 mV/s.

cyclic voltammograms recorded at Pt nanodisk electrodes of different radii immersed in 1.0 M  $N_2H_4$  solution. For a 5.8 nm radius electrode, the peak current  $i_{nb}^p$  at which a  $N_2$  nanobubble nucleates is  $\sim 3.1$  nA, while for a 54 nm radius electrode,  $i_{nb}^p$  increases to  $\sim 17.8$  nA. In contrast, for an electrode above the 90 nm critical radius, the cyclic voltammetric response displays a sigmoidal-shape with large hysteresis between the forward and backward scan (see Supporting Information Figure S3). Why dissolved  $N_2$  molecules do not nucleate into a bubble to cover the entire electrode surface for  $a > \sim 90$  nm is not understood.

Assuming that the voltammetric current exclusively arises from the  $N_2$  electrogeneration and the system is at steady state prior to the liquid-to-gas transition, the measured current can be correlated to the diffusion of  $N_2$  away from the electrode surface using the expression:

$$i_{nb}^p = 4nFD_{N_2}C_{N_2,critical}^s a \quad (4)$$

where  $D_{N_2}$  is the diffusivity of  $N_2$  ( $1.9 \times 10^{-5}$  cm<sup>2</sup>/s),<sup>51</sup> and  $n$  is the number of electrons transferred per formation of a gas molecule ( $= 4$  for  $N_2$ ). Eq 4 relates the  $N_2$  surface concentration,  $C_{N_2,critical}^s$ , to the peak current,  $i_{nb}^p$ , at the moment just prior to bubble nucleation. Eq 4 assumes diffusion of  $N_2$  away from the disk shape electrode surface and is derived from Fick's laws.<sup>40,41</sup> Based on the independent measurements using different disk nanoelectrodes, we find that  $i_{nb}^p$  is proportional to electrode radii, as shown in Figure 6. The slope from the linear plot of  $i_{nb}^p$  vs  $a$  yields the critical surface concentration  $C_{N_2,critical}^s$  of  $0.11 \pm 0.01$  M for  $N_2$ , corresponding to an  $\sim 160$ -fold increase above the saturation value at room temperature and atmospheric pressure ( $\sim 0.69$  mM). Interestingly, such a supersaturation value ( $\sim 160$ ) required to cause  $N_2$  bubble nucleation agrees well with the range of 180–190 reported by Hemmingsen<sup>5–7</sup> and 136 by Finkelstein and Tamir<sup>52</sup> using the classical cavitation method, where the aqueous solutions are equilibrated with  $N_2$  at a high pressure and then suddenly

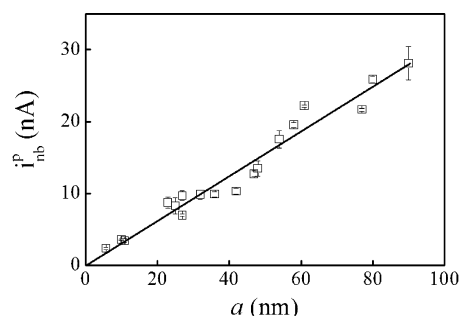
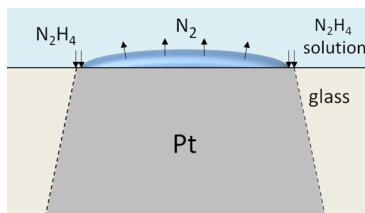


**Figure 6.**  $N_2$  nanobubble peak current,  $i_{nb}^p$ , as a function of nanoelectrode radii for  $N_2$  bubble nucleation in 1.0 M  $N_2H_4$ .

decompressed to observe gas bubbles. These threshold supersaturation concentrations were found for bubbles at the glass/water interface, hence heterogeneous bubble nucleation was likely being observed. On the other hand,  $N_2$  gas supersaturation can also be achieved by the fast decomposition of aqueous nitrite.<sup>53,54</sup> The threshold concentration for homogeneous nucleation in aqueous solution was reported to be 23–100 times the  $N_2$  solubility at 1 atm, depending on the solution ionic strength. However, it is generally accepted that heterogeneous nucleation is substantially faster than homogeneous nucleation due to the pronounced decrease of the critical nucleation energy barrier; this common belief is inconsistent with the above experimentally reported nucleation supersaturation value for  $N_2$  bubble nucleation.

Once formed, we speculate that the stability of a nanobubble should result from a dynamic equilibrium between the  $N_2$  diffusive outflux through the nanobubble/liquid interface (controlled by Henry's law and gas-molecule transfer kinetics) and further  $N_2$  influx into the bubble from gas electrogeneration at the three phase contact line. A similar dynamic equilibrium mechanism for surface nanobubble stabilization has been previously theoretically considered by Brenner,<sup>19</sup> suggesting that the diffusive outflux of gas is compensated by a continuous influx of gas near the contact line, due to gas attraction toward hydrophobic walls. In our study, the influx of gas required to balance the diffusive outflux for a stable nanobubble at an electrode surface can be experimentally measured from the residual current (see Scheme 2). In the following paragraphs, we discuss the stability of a nanobubble at an electrode surface in terms of the measured residual current.

#### Scheme 2. Sketch of Gas Outflux and Influx into the Surface Nanobubble



As shown in Figures 1 and 3, after the formation of a nanobubble, the current decreases to a residual current,  $i_{nb}^r$ . Because of the small size of the Pt disks and the high consistency of the voltammetric results using different electrodes, we believe that the gas nanobubble covers the majority of the surface and that  $N_2H_4$  oxidation associated with the small

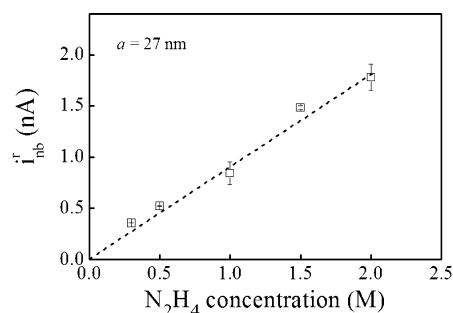


**Figure 7.** Dependence of the residual current,  $i_{nb}^r$ , at 0.8 V from voltammetric response at 100 mV/s for a 27 nm radius disk electrode in  $N_2H_4$  aqueous solutions with different concentrations (0.30, 0.50, 1.0, 1.5, 2.0 M) in Figure 3b.

$i_{nb}^r$  exclusively occurs at the circumference of the Pt disk electrode. In Figure 3b,  $i_{nb}^r$  after bubble formation for a given 27 nm radius nanoelectrode is quite stable, essentially independent of the potential. Figure 7 shows that the  $i_{nb}^r$  obtained in Figure 3b is proportional to the  $N_2H_4$  concentration, suggesting that  $N_2H_4$  transport to the three phase contact line for further gas generation is likely to be the rate-limiting step in establishing the nanobubble dynamic equilibrium. Clearly if  $N_2$  diffusional outflux were rate limiting,  $i_{nb}^r$  would not scale linearly with the  $N_2H_4$  concentration. Surprisingly, in our previous studies of  $H_2$  nanobubble stability, a linear dependence of  $i_{nb}^r$  on proton concentration for a given electrode was not observed.<sup>26,27</sup>

Figure 8 further shows, within experimental error, an approximately linear relationship between  $i_{nb}^r$  at 1.0 M  $N_2H_4$

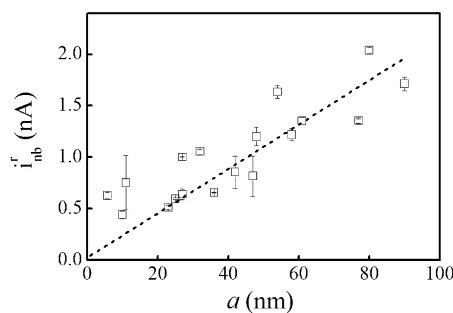


**Figure 8.** Dependence of the residual current,  $i_{nb}^r$ , at 0.8 V from voltammetric response at 100 mV/s as a function of nanoelectrode radii at 1.0 M  $N_2H_4$  solution.

and the radii of nanoelectrodes used for  $N_2$  bubble formation, consistent again with the nanobubble dynamic equilibrium being limited by the size of the three phase contact line available for gas electrogeneration. In summary and, as indicated in Scheme 2, we conclude that the dynamic equilibrium for the nanobubble at the electrode surface is limited by  $N_2$  electrogeneration, which is dependent both on the bulk  $N_2H_4$  concentration and the length of active three phase contact line.

#### CONCLUSIONS

In summary, this study demonstrates that single  $N_2$  nanobubbles can be electrochemically generated from  $N_2H_4$  electrooxidation at Pt nanoelectrodes with radii  $< \sim 90$  nm. The voltammetric current suddenly decreases ( $\sim 93\%$  blockage) as a gas nanobubble forms at the electrode and blocks  $N_2H_4$  transport to the surface. We find that the peak currents at the

moment of bubble nucleation are proportional to the Pt nanoelectrode radii, but independent of  $N_2H_4$  concentration. The critical surface concentration for  $N_2$  nanobubble nucleation is measured to be  $0.11 \pm 0.01$  M, corresponding to  $\sim 160$  times the saturation value at room temperature and atmospheric pressure, consistent with the results of heterogeneous nucleation from classical cavitation methods. After bubble formation, the residual current is proportional to the  $N_2H_4$  concentration as well as the nanoelectrode radii, implying that the nanobubble dynamic equilibrium is limited by the  $N_2$  influx from gas electrogeneration at the three phase contact line. Finally, we suggest that the “blip” current response feature for single Pt nanoparticles collision at a Ni microelectrode, corresponding to the electrocatalytic oxidation of  $N_2H_4$  (reported in ref 35) is unlikely to be due to the  $N_2$  nanobubble formation at the surface of Pt nanoparticle. The  $N_2H_4$  concentration used in that study (8.7 mM) is much lower than the critical concentration required to form a gas nanobubble found in our study (0.30 M).

## ■ ASSOCIATED CONTENT

### 📄 Supporting Information

The Supporting Information is available free of charge on the ACS Publications website at DOI: 10.1021/jacs.5b07147.

Characterization of Pt nanodisk electrodes; dependence of voltammetric responses on immersion time; voltammetric response of a 98 nm radius Pt electrode (PDF)

## ■ AUTHOR INFORMATION

### Corresponding Author

\*white@chem.utah.edu

### Notes

The authors declare no competing financial interest.

## ■ ACKNOWLEDGMENTS

This work was supported by the Office of Naval Research.

## ■ REFERENCES

- (1) Jones, S. F.; Evans, G. M.; Galvin, K. P. *Adv. Colloid Interface Sci.* **1999**, *80*, 27–50.
- (2) Dammer, S. M.; Lohse, D. *Phys. Rev. Lett.* **2006**, *96*, 206101.
- (3) Weathersby, P. K. *J. Appl. Physiol.: Respir., Environ. Exercise Physiol.* **1982**, *53*, 940–946.
- (4) Lubetkin, S. D. *Langmuir* **2003**, *19*, 2575–2587.
- (5) Hemmingsen, E. A. *J. Appl. Phys.* **1975**, *46*, 213–218.
- (6) Gerth, W. A.; Hemmingsen, E. A. *Z. Naturforsch., A: Phys. Sci.* **1976**, *31*, 1711–1716.
- (7) Hemmingsen, E. A. *Nature* **1977**, *267*, 141–142.
- (8) Seddon, J. R. T.; Kooij, E. S.; Poelsema, B.; Zandvliet, H. J. W.; Lohse, D. *Phys. Rev. Lett.* **2011**, *106*, 056101.
- (9) Lou, S.-T.; Ouyang, Z.-Q.; Zhang, Y.; Li, X.-J.; Hu, J.; Li, M.-Q.; Yang, F.-J. *J. Vac. Sci. Technol., B: Microelectron. Process. Phenom.* **2000**, *18*, 2573–2575.
- (10) Zhang, X. H.; Maeda, N.; Craig, V. S. J. *Langmuir* **2006**, *22*, 5025–5035.
- (11) Yang, S.; Dammer, S. M.; Bremond, N.; Zandvliet, H. J. W.; Kooij, E. S.; Lohse, D. *Langmuir* **2007**, *23*, 7072–7077.
- (12) Lauga, E.; Brenner, M. *Phys. Rev. E* **2004**, *70*, 026311.
- (13) Liu, G.; Wu, Z.; Craig, V. S. J. *J. Phys. Chem. C* **2008**, *112*, 16748–16753.
- (14) Plowman, B. J.; Jones, L. A.; Bhargava, S. K. *Chem. Commun.* **2015**, *51*, 4331–4346.
- (15) Zhang, X. H.; Zhang, X. D.; Lou, S. T.; Zhang, Z. X.; Sun, J. L.; Hu, J. *Langmuir* **2004**, *20*, 3813–3815.
- (16) Zhang, L.; Zhang, Y.; Zhang, X.; Li, Z.; Shen, G.; Ye, M.; Fan, C.; Fang, H.; Hu, J. *Langmuir* **2006**, *22*, 8109–8113.
- (17) Yang, S.; Tsai, P.; Kooij, E. S.; Prosperetti, A.; Zandvliet, H. J. W.; Lohse, D. *Langmuir* **2009**, *25*, 1466–1474.
- (18) Ducker, W. A. *Langmuir* **2009**, *25*, 8907–8910.
- (19) Brenner, M. P.; Lohse, D. *Phys. Rev. Lett.* **2008**, *101*, 214505.
- (20) Weijs, J. H.; Lohse, D. *Phys. Rev. Lett.* **2013**, *110*, 054501.
- (21) Zhang, X.; Chan, D. Y. C.; Wang, D.; Maeda, N. *Langmuir* **2013**, *29*, 1017–1023.
- (22) Westerheide, D. E.; Westwater, J. W. *AIChE J.* **1961**, *7*, 357–362.
- (23) Dapkus, K. V.; Sides, P. J. *J. Colloid Interface Sci.* **1986**, *111*, 133–151.
- (24) Gabrielli, C.; Huet, F.; Keddam, M. *J. Appl. Electrochem.* **1989**, *19*, 617–629.
- (25) Nakabayashi, S.; Shinozaki, R.; Senda, Y.; Yoshikawa, H. Y. *J. Phys.: Condens. Matter* **2013**, *25*, 184008.
- (26) Luo, L.; White, H. S. *Langmuir* **2013**, *29*, 11169–11175.
- (27) Chen, Q.; Luo, L.; Faraji, H.; Feldberg, S. W.; White, H. S. *J. Phys. Chem. Lett.* **2014**, *5*, 3539–3544.
- (28) Chen, Q.; Luo, L.; White, H. S. *Langmuir* **2015**, *31*, 4573–4581.
- (29) Rosca, V.; Koper, M. T. M. *Electrochim. Acta* **2008**, *53*, 5199–5205.
- (30) Aldous, L.; Compton, R. G. *Phys. Chem. Chem. Phys.* **2011**, *13*, 5279–5287.
- (31) Chen, C.-H.; Jacobse, L.; McKelvey, K.; Lai, S. C. S.; Koper, M. T. M.; Unwin, P. R. *Anal. Chem.* **2015**, *87*, 5782–5789.
- (32) Sanabria-Chinchilla, J.; Asazawa, K.; Sakamoto, T.; Yamada, K.; Tanaka, H.; Strasser, P. *J. Am. Chem. Soc.* **2011**, *133*, 5425–5431.
- (33) Xiao, X.; Fan, F.-R. F.; Zhou, J.; Bard, A. J. *J. Am. Chem. Soc.* **2008**, *130*, 16669–16677.
- (34) Kwon, S. J.; Bard, A. J. *J. Am. Chem. Soc.* **2012**, *134*, 10777–10779.
- (35) Jung, A. R.; Lee, S.; Joo, J. W.; Shin, C.; Bae, H.; Moon, S. G.; Kwon, S. J. *J. Am. Chem. Soc.* **2015**, *137*, 1762–1765.
- (36) Wakerley, D.; Guell, A. G.; Hutton, L. A.; Miller, T. S.; Bard, A. J.; Macpherson, J. V. *Chem. Commun.* **2013**, *49*, 5657–5659.
- (37) Guo, Z.; Percival, S. J.; Zhang, B. *J. Am. Chem. Soc.* **2014**, *136*, 8879–8882.
- (38) Gilbert, E. C. *J. Am. Chem. Soc.* **1929**, *51*, 2744–2751.
- (39) Zhang, B.; Zhang, Y.; White, H. S. *Anal. Chem.* **2004**, *76*, 6229–6238.
- (40) Saito, Y. *Rev. Polarogr.* **1968**, *15*, 177–182.
- (41) Bard, A. J.; Faulkner, L. R. *Electrochemical Methods: Fundamentals and Applications*; 2nd ed.; John Wiley & Sons: New York, 2001.
- (42) Kuwana, T.; Bubltz, D. E.; Hoh, G. *J. Am. Chem. Soc.* **1960**, *82*, 5811–5817.
- (43) Maloy, J. T. In *Standard Potentials in Aqueous Solutions*; Bard, A. J., Parsons, R., Jordan, J., Eds.; Dekker: New York, 1985; pp 127.
- (44) Nishihara, C.; Raspini, I. A.; Kondoh, H.; Shindo, H.; Kaise, M.; Nozoye, H. *J. Electroanal. Chem.* **1992**, *338*, 299–316.
- (45) Gómez, R.; Orts, J. M.; Rodes, A.; Feliu, J. M.; Aldaz, A. J. *Electroanal. Chem.* **1993**, *358*, 287–305.
- (46) Karp, S.; Meites, L. *J. Am. Chem. Soc.* **1962**, *84*, 906–912.
- (47) Szpak, S.; Stonehart, P.; Katan, T. *Electrochim. Acta* **1965**, *10*, 563–583.
- (48) Rosca, V.; Duca, M.; de Groot, M. T.; Koper, M. T. M. *Chem. Rev.* **2009**, *109*, 2209–2244.
- (49) Bard, A. J. *Anal. Chem.* **1963**, *35*, 1602–1607.
- (50) Kleijn, S. E. F.; Lai, S. C. S.; Miller, T. S.; Yanson, A. I.; Koper, M. T. M.; Unwin, P. R. *J. Am. Chem. Soc.* **2012**, *134*, 18558–18561.
- (51) Cussler, E. L. *Diffusion: Mass Transfer in Fluid Systems*; 2nd ed.; Cambridge University Press: New York, 1997.
- (52) Finkelstein, Y.; Tamir, A. *AIChE J.* **1985**, *31*, 1409–1419.
- (53) Rubin, M. B.; Noyes, R. M.; Smith, K. W. *J. Phys. Chem.* **1987**, *91*, 1618–1622.
- (54) Rubin, M. B.; Noyes, R. M. *J. Phys. Chem.* **1992**, *96*, 993–1000.